The Influence of a Capping Inversion on the Dynamic and Convective Instability of a Boundary Layer Model with Shear

EARL E. GOSSARD

Wave Propagation Laboratory, NOAA, Boulder, Colo. 80302

WILLIAM R. MONINGER

Coe College, Cedar Rapids, Iowa 52402

(Manuscript received 31 March 1975, in revised form 15 July 1975)

ABSTRACT

The dynamic instability and the kinematics of a multi-layer, shear model of a convective boundary layer are analyzed. Important features of the model include a capping temperature inversion that may or may not be accompanied by a wind discontinuity, a surface-based superadiabatic layer, and a statically stable upper atmosphere. It is shown that the capping inversion can result in a relatively narrow band of dynamically unstable wavenumbers that depend on shear layer thickness, implying a strong selection of scale in growing disturbances. The influence of the various model parameters on selection of the "most unstable" scales is shown and their corresponding propagation velocities are calculated.

A simple form of the model is also used to examine the characteristics of the convectively unstable modes. It is found that two-dimensional disturbances aligned transverse to the wind shear are most dynamically unstable, whereas two-dimensional disturbances parallel to the wind shear are most convectively unstable.

The vorticity and general kinematics of the disturbances are affected in an important way by the presence of a critical level within the height range occupied by the disturbance.

1. Introduction

The current literature contains innumerable papers on the dynamic and kinematic structure of the convective boundary layer. These are mostly numerical investigations requiring the use of high-speed computers. Many have concerned themselves with Ekman layer instabilities in which wind profiles representative of an Ekman planetary boundary layer are assumed. A few examples of studies of this kind are those of Lilly (1966), Brown (1970, 1972), Kaylor and Faller (1972), Gallagher and Mercer (1965), Maslowe and Thompson (1971) and Deardorff (1965). Observational data have been provided by LeMone (1973). There is also a large literature on such subjects as numerical modeling of severe storms, cloud physics, and wet convection.

In addition to the investigations listed above, which are primarily numerical in nature, various analytic studies of simple models have been carried out. A few of these include the work of Case (1960), Kuo (1963) and Asai (1970) who analyzed the stability of two- and three-dimensional disturbances in a thermally unstable shear flow; Ramm and Warren (1963) who examined the dispersive character of impulsively generated waves in two-layer models with a surface-based adiabatic layer under shear; and Gossard (1974) who investigated the dynamic stability of both surface-based and elevated adiabatic shear layers within a stable atmosphere.

In some ways analytic models have advantages over numerical models, although numerical models can, of course, be more complicated and therefore can be more realistic. Analytic approaches often provide more physical insight, and they can usually be parameterized in a simple enough way so that the contribution of the various elements composing the model can be seen more clearly. We consider that much of the value of the model we have analyzed lies in the insight it can provide for numerical models that may include viscosity, nonlinear effects, and gaseous and liquid water.

Our model differs from others listed above in that it includes a capping temperature inversion, a surface-based superadiabatic layer, and a wind shear layer of varying height above the ground. Our model is three-dimensional, and we examine not only the conditions for dynamic instability but the kinematics of the initially most unstable disturbances and the influence of a critical level on the velocity fields and vorticity. As in most of the analytic studies listed above, our approach is to solve the boundary value problem by the method of normal modes.

2. The model

Our primary purpose is to examine the effects of a capping inversion on the dynamic stability of a boundary layer under shear. We choose to study a model

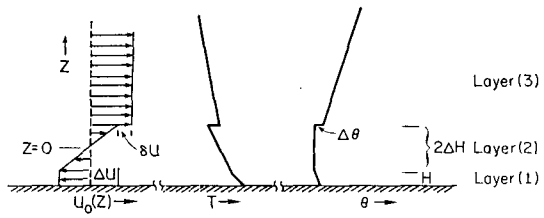

FIG. 1. The model. θ is potential temperature.

(Fig. 1) in which the shear layer is adiabatic because it has mathematically simple solutions such that fairly complicated layered models, including a capping inversion, can be synthesized by satisfying the dynamic and kinematic interfacial boundary conditions. Such a model is not representative of steady, horizontally homogeneous conditions because the large momentum flux that accompanies strong mixing in a shear layer will tend to erase the shear unless sources and sinks of momentum external to the system are maintained. Therefore, we do not claim this to be a general or typical representation of real boundary layers, but we do believe that real environments resemble it often enough so that it is worthwhile working out the consequences of the model and examining the way the various parameters of the model affect its dynamic instability. Of course it is unlikely in nature that the shear will ever coincide with a precisely adiabatic layer. In reality a transition zone between a superadiabatic region below and a somewhat stable region above, as seen in Fig. 2, is more likely. We hope the essential physics is not lost by representing the transition zone as an adiabatic layer. Beneath the shear layer we choose a neutral or superadiabatic layer without shear (except, of course, in a thin layer next to the ground which we neglect). In the analytic development we allow for a temperature discontinuity at the base of the shear layer as well as at the top, but in the numerical calculations we have assumed the lower discontinuity to be zero as shown in the schematic representation of our model in Fig. 1.

We believe the model may sometimes also be representative of environments that can lead to large-scale convective development and severe storms. Fig. 2 shows such an example. The "capping" inversion at 500 mb in this example is due to subsidence and is a common feature of soundings in this area and season. It is typically accompanied by an abrupt decrease in humidity with height. In the afternoon of the case shown, widespread cumulonimbus development occurred with damaging hail. The progression of the cells was from southwest to northeast which is in the direction of principal shear (x,z plane) having an azimuth of 230°.

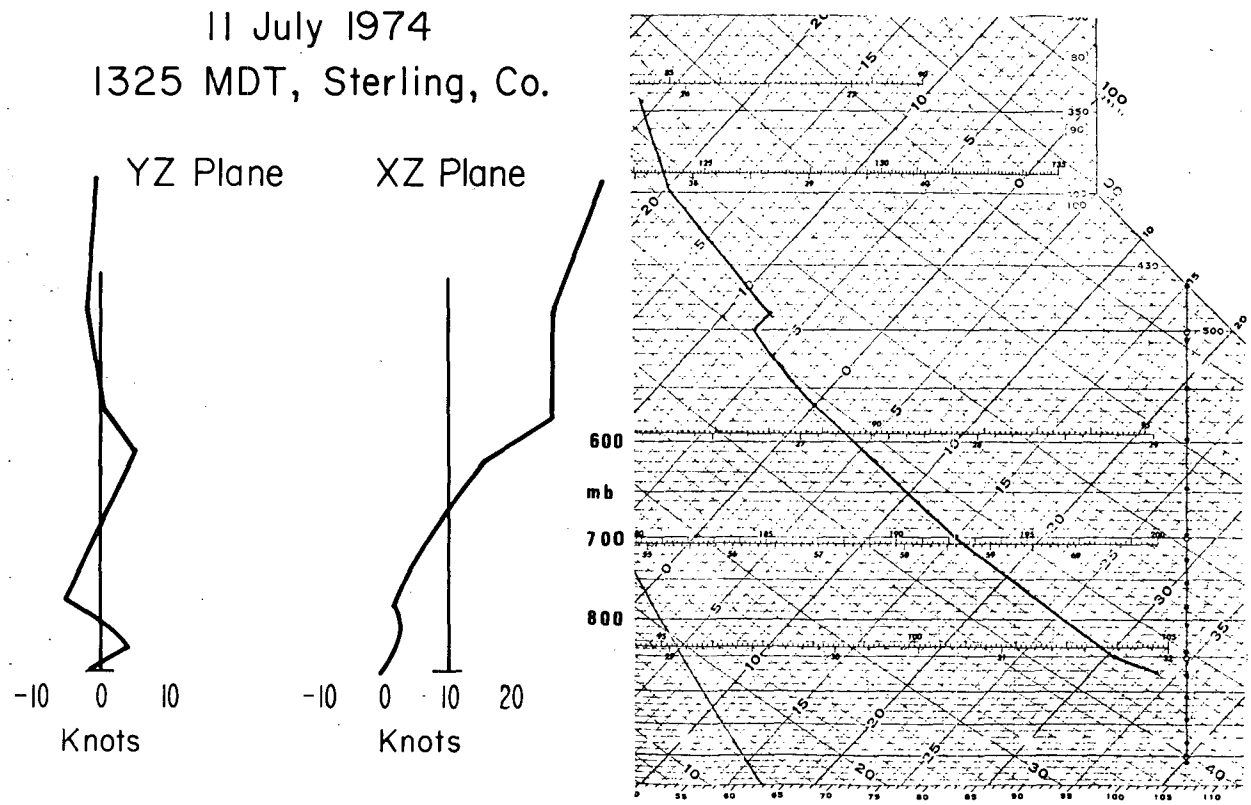

FIG. 2. Wind and temperature soundings made in severe storm conditions. Large-scale cumulonimbus development occurred in the afternoon. Cells moved from southwest to northeast. The x,z plane (the plane of principal shear) was oriented 230° in azimuth. Wind and temperature are plotted to the same height scale.

Clearly, the presence of the dynamic instability we discuss is not sufficient to ensure the development of convective storms. Factors such as the available moisture supply in the low-level air as well as convergence and vorticity in the mesoscale flow patterns will largely determine whether the "trigger" we propose will be effective in initiating large-scale convection.

The key characteristics of the model that lead to the important consequences are the inflection point in the wind profile which is the primary cause of the dynamic instability, and the capping inversion that confines the instability to a relatively narrow band of wavenumbers.

3. The linearized equations including shear

For a basic flow with vertical shear ($\partial u_0/\partial z$) in the x direction, the linearized equations of motion, continuity and energy conservation for adiabatic processes are

$$\frac{D}{Dt}\left(\frac{\partial u}{\partial x}\right)+\frac{1}{\rho_0}\frac{\partial^2 p}{\partial x^2}+\frac{\partial u_0}{\partial z}\frac{\partial w}{\partial x}=0, \tag{1}$$

$$\frac{D}{Dt}\left(\frac{\partial}{\partial y}\right)+\frac{1}{\rho_0}\frac{\partial^2 p}{\partial y^2}=0, \tag{2}$$

$$\frac{Dw}{Dt}+\frac{1}{\rho_0}\frac{\partial p}{\partial z}+g\frac{\rho}{\rho_0}=0, \tag{3}$$

$$\frac{D\rho}{Dt}+w\frac{\partial \rho_0}{\partial z}+\rho_0\nabla\cdot\mathbf{v}=0, \tag{4}$$

$$\frac{D\rho}{Dt}+w\frac{\partial \rho_0}{\partial z}=\frac{1}{c^2}\left(\frac{Dp}{Dt}+w\frac{\partial p_0}{\partial z}\right), \tag{5}$$

where u, v, w, ρ, p are small perturbations of the x, y, z components of wind, and of density and pressure. Zero subscripts indicate unperturbed quantities, and c is sound velocity. We have chosen the x direction as the direction of the undisturbed flow, so $v_0=w_0=0$ and the operator $D/Dt=\partial/\partial t+u_0(z)\partial/\partial x$.

It is convenient first to eliminate ρ between Eqs. (4) and (5). We then adopt the transformation

$$U,\ V,\ W,\ P^{-1}=(\rho_0/\rho_s)^{\frac{1}{2}}[u,\ v,\ w,\ p^{-1}], \tag{6}$$

where $\rho_0(z)$ is the distribution of the unperturbed density with height, and ρ_s is the density at some reference level such as the surface. The resulting partial differential equations are linear and homogeneous, and a solution representing one of the simplest forms of three-dimensional disturbance is

$$U,\ V,\ W,\ P=\tfrac{1}{2}[U(z),\ V(z),\ W(z),\ P(z)]\times[\exp i(kx+ly-\sigma t)\pm\exp i(kx-ly-\sigma t)], \tag{7}$$

which requires the following phasing of the variables:

$$P=P(z)\cos ly\sin(kx-\sigma t) \tag{8}$$

$$U=U(z)\cos ly\sin(kx-\sigma t) \tag{9}$$

$$V=V(z)\sin ly\cos(kx-\sigma t) \tag{10}$$

$$W=W(z)\cos ly\cos(kx-\sigma t). \tag{11}$$

Elimination of $P(z)$, $U(z)$ and $V(z)$ leads to the ordinary differential equation in $W(z)$:

$$\frac{d^2W(z)}{dz^2}-\left\{m^2-\frac{u_0''k}{[C-u_0(z)]}-\frac{(Nm/k)^2}{[C-u_0(z)]^2}\right\}W(z)=0, \tag{12}$$

where $m^2\equiv k^2+l^2$, $u_0''\equiv d^2u_0/dz^2$. The phase velocity in the x direction is $C=\sigma/k$. In deriving Eq. (12), we have defined $N^2\equiv -g(\rho_0^{-1}d\rho/dz+g/c^2)=(g/\theta_0)d\theta/dz$, where N is the Väisälä-Brunt frequency (Väisälä, 1925; Brunt, 1927) and θ is potential temperature. Furthermore, we have neglected the quantity $(2\rho_0)^{-1}d\rho_0/dz+g/c^2$ compared with the operator $\partial/\partial z$ applied to the field variables, and we have assumed $C\ll c$. This is a form of the Boussinesq approximation and implies that we have assumed the scale depth of the atmosphere to be large compared with the scale depth of the disturbance. Eq. (12) is exactly the same as the wave equation for a two-dimensional disturbance except that k has been replaced by m and N has been replaced by (Nm/k).

From (7) we see that $D/Dt=-i\sigma+iku_0(z)\equiv -i\omega(z)$, which defines the intrinsic frequency $\omega=k[C-u_0(z)]$, where $C=\sigma/k$ is the velocity of the disturbance in the x direction. Thus ω can become zero at a "critical level" where $u_0=C$.

Then in terms of ω, $W(z)$ is related to the other variables as

$$U(z)=-\frac{k}{m^2}\left(\frac{\partial}{\partial z}-\frac{k}{\omega}\beta-\frac{l^2}{k^2}\right)W(z), \tag{13}$$

$$V(z)=-\frac{l}{m^2}\left(\frac{\partial}{\partial z}+\beta-\frac{k}{\omega}\right)W(z), \tag{14}$$

$$P(z)=-\rho_s\frac{\omega}{m^2}\left(\frac{\partial}{\partial z}+\beta-\frac{k}{\omega}\right)W(z), \tag{15}$$

where $\beta\equiv\partial u_0/\partial z$.

If the coefficient in Eq. (12) is constant, it has very simple solutions which are some combination of exponentials. The coefficient is constant if both u_0''/ω and $(N/\omega)^2$ are constant or zero, but (12) will have annoying singularities at any height where $\omega=0$. In 1880 Lord Kelvin discussed this "disturbing infinity in Lord Rayleigh's solution for waves in a plane vortex stratum." He pointed out that if u_0'' is zero (and the fluid is homogeneous, i.e., $N=0$) "we evade entirely the consideration of this infinity." The simple solutions then apply, and Kelvin proceeded to deduce the now famous Kelvin's cat's eye pattern at the critical level from purely kinematic considerations.

In the model we analyze here, the atmosphere will be assumed to be adiabatic and the wind shear to be constant in the layer containing the critical level. As pointed out by Kelvin, we thus avoid the difficulty with singularities if we deal with vertical velocity. The simple solutions then apply and we can synthesize fairly complicated models by satisfying appropriate boundary conditions between the several layers of the model. However, although W is well behaved, the particle displacement is given by W/ω and would thus become infinite as ω goes to zero. Consequently, Kelvin's artifice does not allow us to "evade entirely" the problem of infinities at the critical level. However, confidence in the approach may be derived from the "reasonable" results deduced from such models as those examined by Taylor (1931), Goldstein (1931), Howard (1963), Holmboe (1962) and Gossard (1974). The singularities arise primarily because of the absence of viscosity in our model, and complete justification of the results must be found in a comparison with results found in models in which viscosity is included. Hazel (1967) solved numerically the full sixth-order differential equation including viscosity for flux-matching conditions across the critical level. He compared his results with those found for a model without viscosity by Booker and Bretherton (1967) and concluded that the results were identical within the limits of numerical truncation errors. We will now proceed to analyze a model made up of layers in which $u_0''=0$ and $(N/\omega)^2$ is either zero or constant.

4. The boundary conditions

To proceed with the solution of (12) for the multilayered model shown in Fig. 1, the eigensolutions which satisfy certain boundary conditions must be found.

At the surface, assumed to be level and rigid, $w=0$. At the interfaces between layers 1 and 2 and between 2 and 3, we satisfy the kinematic conditions $w_1=w_2$, $w_2=w_3$; and the dynamic conditions $p_{T1}=p_{T2}$ and $p_{T2}=p_{T3}$, where p_T is total pressure. The latter conditions can most conveniently be applied by requiring continuity in dp_T/dt where

$$\frac{dp_T}{dt}=\frac{Dp}{Dt}+w\frac{\partial p_0}{\partial z}=\left(\frac{\rho_0}{\rho_s}\right)^{\frac{1}{2}}\left(\frac{DP}{Dt}-\rho_s gW\right),$$

in which we have used the hydrostatic relation $\partial p_0/\partial z=-\rho_0 g$ and the transformation (6). If there is a discontinuity in the wind profile, the conditions of continuity in W and dp_T/dt are only exactly true in the long-wavelength (or small-amplitude) limit (see Gossard and Hooke, 1975). A somewhat more precise statement is that the displacement (and therefore W/ω) is continuous across boundaries. However, this condition is applied at the undisturbed position of the interface and therefore it also is only true in the small-amplitude limit. The degrees of approximation are comparable and either set of conditions leads to the same result. If we choose the interface to be the reference level of ρ_s, we have at the interface $\rho_{01}=\rho_{s1}$ and $\rho_{02}=\rho_{s2}$ so we require continuity in $DP/Dt-\rho_s gW$ across the interfaces. Letting β be the shear, the basic equations (8), (11) and (15) yield the differential relation

$$\frac{DP}{Dt}=-\frac{\rho_s\omega^2}{m^2}\left(\frac{\partial}{\partial z}+\frac{k}{\omega}\beta\right)W,$$

so that the dynamic boundary condition expressed in terms of W requires continuity of

$$\rho_s\frac{\omega^2}{m^2}\left(\frac{\partial}{\partial z}+\frac{k}{\omega}\beta\right)W-\rho_s gW. \tag{16}$$

Therefore, both the kinematic and dynamic boundary conditions at the interfaces can be satisfied by restrictions on W only. Because $\omega=k[C-u_0(z)]$ for a model with vertical shear, we readily see from Fig. 1 that

$$\left.\begin{aligned} &u_0(z)=-\Delta u, && \omega=k(C+\Delta u), && z<-\Delta H\\ &u_0(z)=\frac{\Delta u}{\Delta H}z=\beta z, && \omega=k\left(C-\frac{\Delta u}{\Delta H}z\right), && -\Delta H<z<\Delta H\\ &u_0(z)=\Delta u+\delta u, && \omega=k(C-\Delta u-\delta u), && z>\Delta H \end{aligned}\right\},$$

so that $\omega_1/\beta=(k/m)\alpha(\xi+1)$, $\omega_3/\beta=(k/m)\alpha(\xi-1-\delta)$, where $\beta=\Delta u/\Delta H$, $\alpha=m\Delta H$, $\xi=C/\Delta u$, and $\delta=\delta u/\Delta u$.

Finally, we require that the modified vertical velocity W not become infinite at infinity.

5. The eigensolutions

If we choose the origin to be at the center of the shear layer, i.e., at $H+\Delta H$, solutions which satisfy the boundary conditions in the various layers are:

$$W_1=W_H\frac{\sinh\gamma_1(z+H+\Delta H)}{\sinh\gamma_1 H} \tag{17}$$

$$W_2=W_H\frac{\sinh mz+A\cosh mz}{-\sinh m\Delta H+A\cosh m\Delta H}$$

$$\equiv W_{H+2\Delta H}\frac{\sinh mz+A\cosh mz}{\sinh m\Delta H+A\cosh m\Delta H} \tag{18}$$

$$W_3=W_{H+2\Delta H}\exp[-\gamma_3(z-\Delta H). \tag{19}$$

Satisfying the condition (16) at the lower boundary of the shear layer we find for A that

$$A=\frac{(\xi+1)^2(\alpha_1\tanh\alpha+\alpha)-(\xi+1)\tanh\alpha-R'(m/k)^2\tanh\alpha}{(\xi+1)^2(\alpha_1+\alpha\tanh\alpha)-(\xi+1)-R'(m/k)^2}; \tag{20}$$

and from the condition at the upper boundary

$$A=-\frac{\alpha_3(\xi-1-\delta)^2\tanh\alpha+\alpha(\xi-1)^2+(\xi-1)\tanh\alpha-R(m/k)^2\tanh\alpha}{\alpha_3(\xi-1-\delta)^2+\alpha(\xi-1)^2\tanh\alpha+(\xi-1)-R(m/k)^2}, \tag{21}$$

where $\xi=C/\Delta u=(\sigma/\beta\alpha)\ (m/k)$, $C=\sigma/k$ is the velocity of the disturbance, $\alpha_1=\gamma_1\Delta H$ ctnh $\gamma_1 H$, $\alpha_3=\gamma_3\Delta H$,

$$\gamma_3=[1-(N_3/\beta)^2/(\omega_3/\beta)^2]^{\frac{1}{2}}m,$$

$$\gamma_1=[1-(N_1/\beta)^2/(\omega_1/\beta)^2]^{\frac{1}{2}}m,$$

$$R=-\frac{g\Delta\rho}{\rho_0}\frac{\Delta H}{\Delta u^2}\approx\frac{g\Delta\theta}{\theta_0}\frac{\Delta H}{\Delta u^2}$$

where θ is potential temperature, and $\Delta\theta$ the potential temperature discontinuity at the top of the shear layer, and

$$R'=\frac{g\Delta\theta'}{\theta_0}\frac{\Delta H}{\Delta u^2},$$

where $\Delta\theta'$ is the potential temperature discontinuity at the base of the shear layer ($\Delta\theta'=0$ in Fig. 1).

Equating (20) and (21) yields the eigenvalue curves for the model, i.e., the relation between ξ and α for assumed values of N_3/β, δ, R and $H/\Delta H$. It is similar to Eq. (16) in the paper by Gossard (1974) except that we here express the relations in terms of hyperbolic rather than exponential functions. We have generalized the earlier model by including a wind discontinuity δu at the top of the shear layer and by permitting the lower layer to be superadiabatic.

Because $\omega\propto k$, we see in Eqs. (12), (20) and (21) that buoyancy terms in N^2 and R always appear multiplied by $(m/k)^2\equiv 1+l^2/k^2$. Therefore, the three-dimensional model is derivable from the two-dimensional case simply by introducing a modified Väisälä-Brunt frequency and a modified R, which are the unmodified quantities multiplied by m/k and $(m/k)^2$ respectively. It is immediately seen from Eq. (12) that the buoyancy term is minimum for the two-dimensional case, i.e., $m=k$. Therefore, for a statically stable layer ($N^2>0$), the two-dimensional model is least stable because the stabilizing effect of the buoyancy term is minimum. However, when $N^2<0$, the destabilizing effect of buoyancy becomes larger as l/k becomes larger, so there will be a tendency for disturbances oriented along the x direction (parallel to the direction of shear) to grow most rapidly.

It should also be noted that the conditions (20), (21) apply to a two-dimensional perturbation propagating at an angle to the shear as well as to the three-dimensional disturbance described by Eq. (7).

6. The unstable roots

It is of primary interest to inquire what value of the frequency σ has the largest imaginary component and to determine the associated value of α. This will indicate the scale of the most rapidly growing disturbance. (Actually, since $\alpha=m\Delta H$, it indicates the ratio of scale to layer thickness.) We have therefore plotted the dispersion relation in terms of σ rather than ξ, noting that $\sigma/\beta=\alpha\xi k/m$. In this kind of analysis it is presumed that the initially most rapidly growing disturbance will remain the dominant scale after the original approximations of the small-amplitude, inviscid theory are no longer applicable.

The real roots of Eqs. (20), (21) can be easily found using any modern, programmable desk calculator. The complex roots were found by use of a high-speed computer and a search algorithm modified from one originally written by Lewis (1966; see Moninger, 1974).

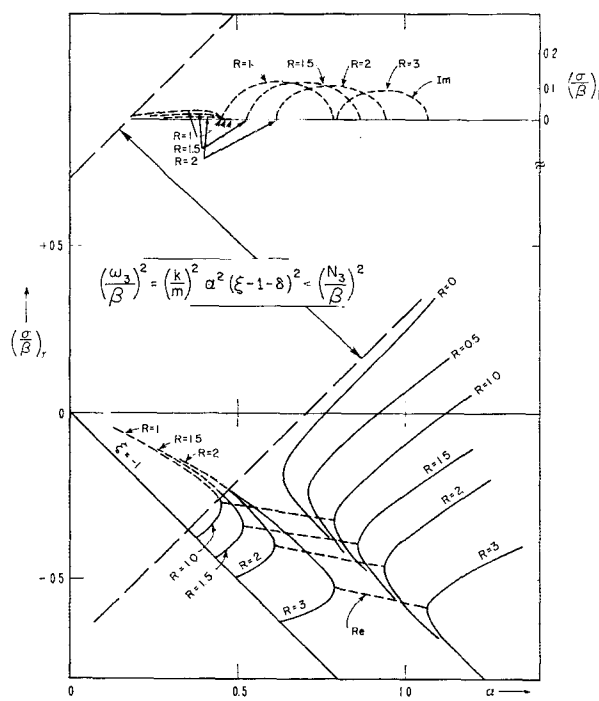

FIG. 3. Example of eigenvalue curves for the conditions shown on the figure. Solid lines represent loci of real roots; short dashed lines represent the real and imaginary parts of complex roots. Long dashed lines indicate boundaries within which $|\omega|<N_3$. Top frame: The imaginary parts are shown in the top frame of the figure. There are generally two domains of nonzero imaginary part (indicated by curved arrows) separated by a region of real roots. Both positive and negative values of the imaginary part are solutions but they have been arbitrarily plotted as positive. Bottom frame: Hyperbola-like solid curves and the straight line sloping down to the right are loci of real roots. The interval of α between noses of branches of hyperbolas is the domain of dynamic instability and yield the stability boundaries plotted in the next figures. The model is two-dimensional so $m=k$; $H/\Delta H=1$, $\delta=0$, $(N_3/\beta)^2=0.5$, $(N_1/\beta)^2=-0.1$.

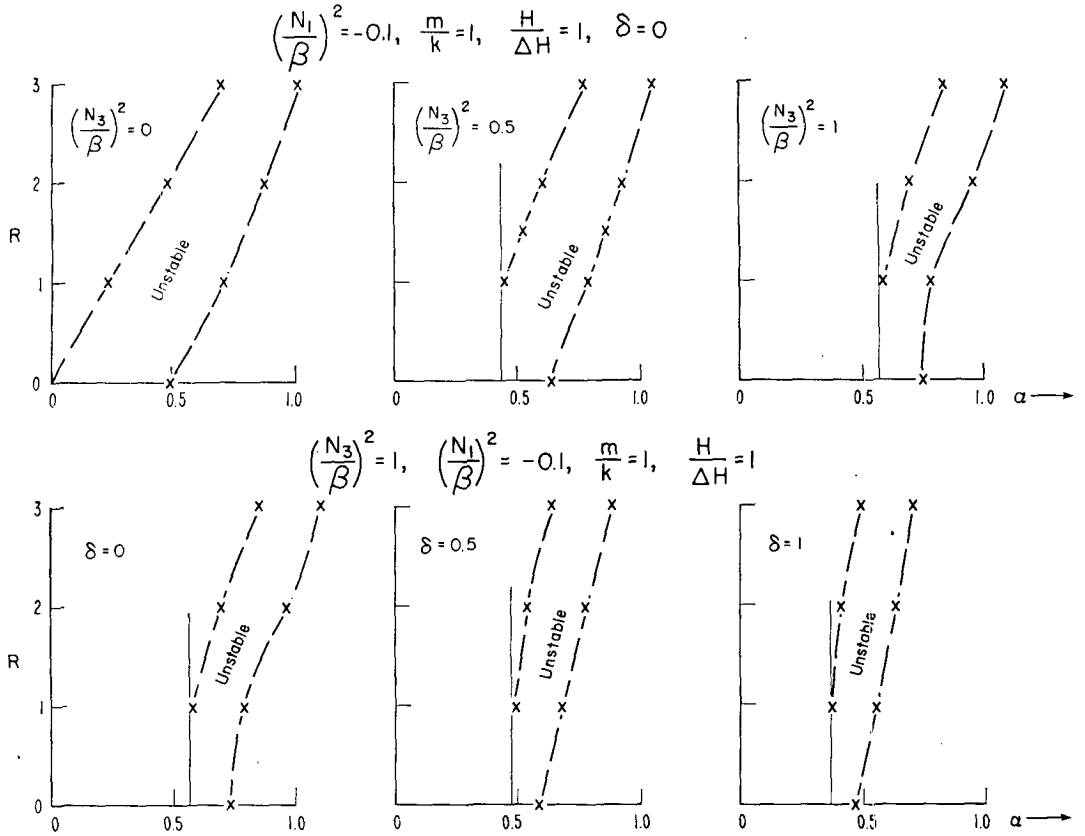

FIG. 4. Stability boundaries for various values of model parameters for the two-dimensional case, i.e., $m=k$. The figure demonstrates the influence of static stability in the upper layer of the model and the effect of a wind discontinuity at the top of the shear layer. $\delta=\delta u/\Delta u$. Points actually calculated are shown as ×'s. γ_3 is not real for values of α less than the intercept with the thin vertical line.

a. Bandwidth of the instability

Fig. 3 shows an example of the loci of the roots found by equating (20) and (21) for conditions indicated in the caption. Purely real roots are indicated by solid lines. The real and imaginary parts of complex roots are indicated by short dashes. Above the lower line composed of long dashes, the radicand of γ_3 becomes negative, i.e., $(k/m)^2\alpha^2(\xi-1-\delta)^2<(N_3/\beta)^2$. Physically, this indicates the existence of vertical fluxes of energy and momentum resulting from internal gravity waves in the upper layer of the model and implies relative dissipation of disturbances in this domain of the figure due to leakage of energy away from the shear layer. For R greater than about unity, this domain of complex roots in Fig. 3 is separated from that representing dynamic instability. (Note separation of arrowheads showing the "foot" of the curves for $R=1.5$ and $R=2$ in the upper frame of the figure.) At smaller values of R, the two domains merge. Above the upper line of long dashes the radicand of γ_3 again becomes positive. If roots exist in this domain, such high-speed disturbances would have their energy trapped within the lower regions of the model like those in the domain below the lower dashed line.

The loci of the real part of the complex roots in the unstable domain link the noses of the branches of the hyperbola-like curves representing the real roots. This region delineates the instability boundaries, and these instability boundaries are shown in Figs. 4–6 for many combinations of the various parameters describing the model.

We see that there is, in general, a relatively narrow band of unstable wavenumbers. The narrow-band character of the instability is a result of the temperature discontinuity at the top of the shear layer, and the scale and bandwidth of the unstable disturbances depend significantly on R. The width of the unstable band shrinks to zero as H tends toward zero because when $H=0$ there is no inflection point in the velocity profile (see Fig. 1). Because we have chosen a model in which the stability (described by N) is precisely zero in the shear layer, there is instability for some scales at all values of R. The width of the band of unstable wavenumbers also depends importantly on the intensity of the superadiabatic layer as described by N_1/β, the stability of the upper atmosphere, N_3/β, and the height H of the base of the shear layer. As seen from Fig. 6, the lower layer need not be superadiabatic for this kind of

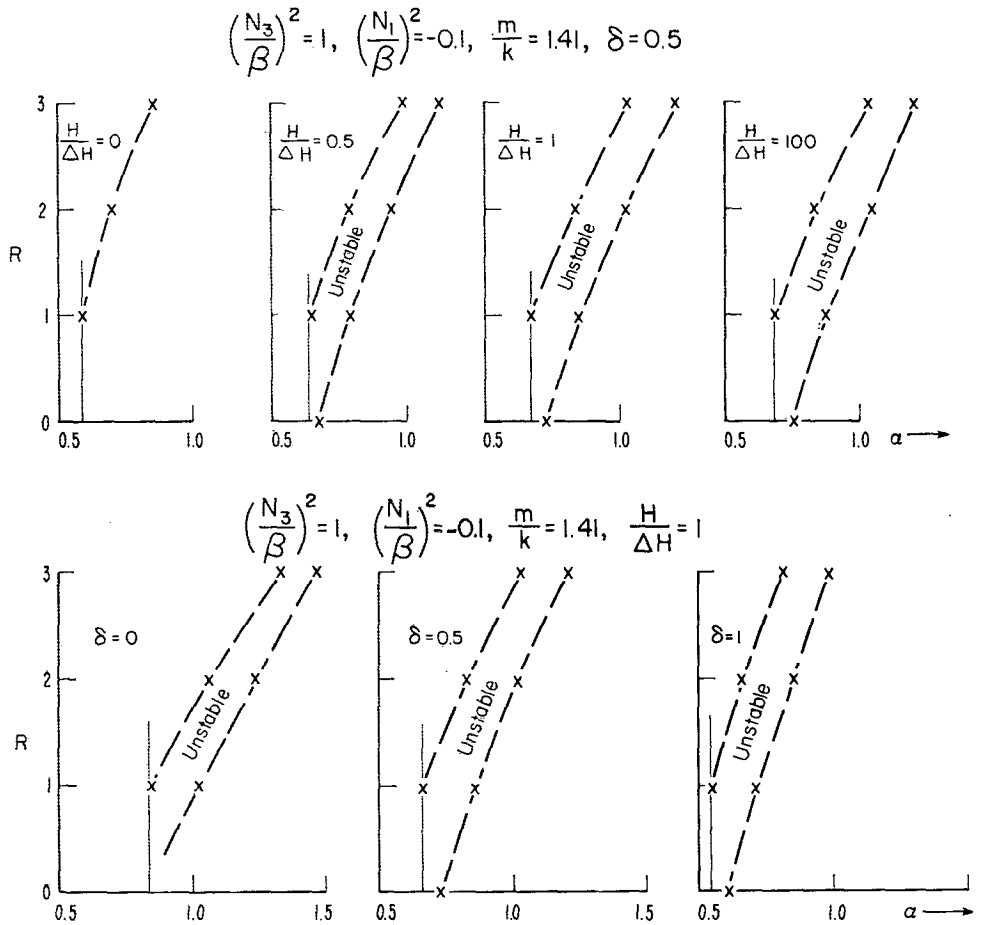

FIG. 5. Stability boundaries for various values of model parameters for the three-dimensional case in which $k=l$, i.e., $m=1.41k$. The figure demonstrates the influence of height of the base of the shear layer above the surface and the influence of a wind discontinuity at the top of the shear layer. Otherwise see caption for Fig. 4.

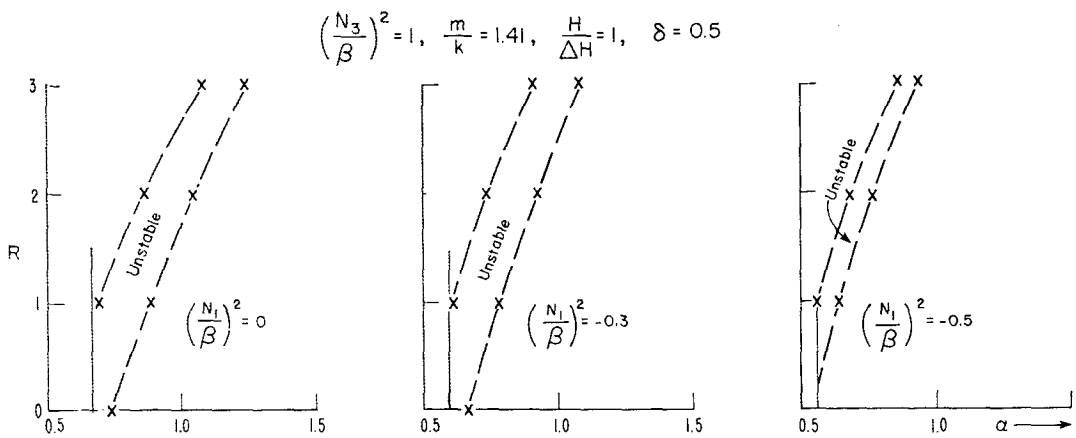

FIG. 6. Stability boundaries for various values of model parameters for the three-dimensional case, showing the influence of intensity of the superadiabatic surface layer. Otherwise see captions for Figs. 4 and 5.

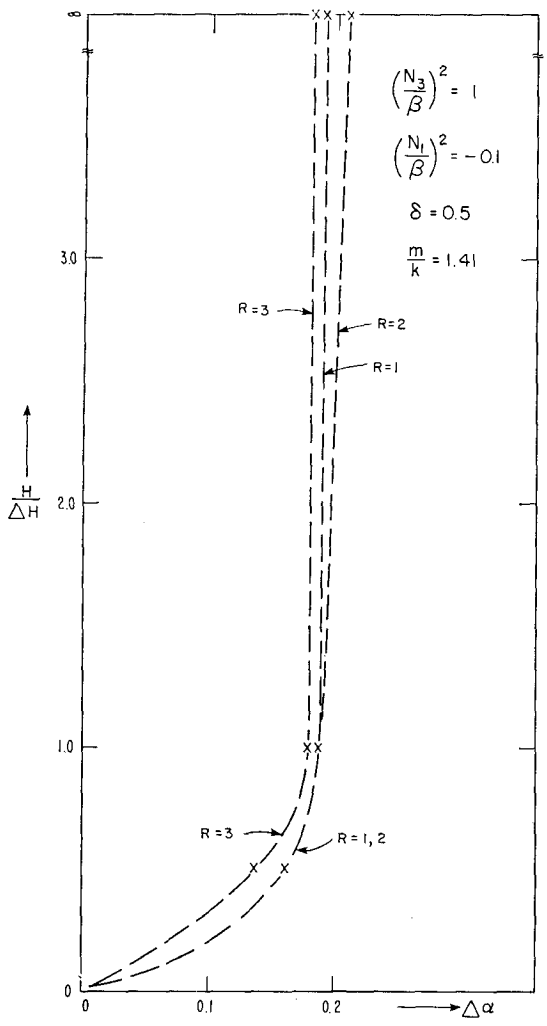

FIG. 7. Dependence of bandwidth of unstable disturbances, $\Delta\alpha$, on the ratio of the height of the base of the shear layer to its half-thickness ΔH.

instability to occur. In fact, below $(N_1/\beta)^2 = -0.5$ the bandwidth of instability shrinks to zero at $m/k = 1.41$. The bandwidth dependence on H and R is shown in Fig. 7. The main effect of δ is to shift the position of the band.

b. *Propagation velocity*

Relative to the background wind, the velocity of the most unstable disturbance is given by the real part of ξ and is shown plotted in Figs. 8–11 for various combinations of model parameters. We see that the disturbance propagates more slowly as the base of the shear layer lowers, becoming equal to the ambient velocity of the wind in the lower layer as H shrinks to zero. Likewise, the propagation velocity decreases as the lowest layer becomes more intensely superadiabatic. The propagation velocity becomes that of the wind in the lower layer when $(N_1/\beta)^2$ reaches approximately -0.5. Typically, values of $C/\Delta u$ are in the vicinity of -0.6, which means that the disturbance moves considerably slower than the average background wind, i.e., about 0.4 of the wind speed at the center of the shear layer.

c. *Convective instability and roll orientation*

Until now, we have considered only dynamic instability. However, if $(N_1/\beta)^2$ is negative, solutions representing convective instability also exist. As $(N_1/\beta)^2$ becomes increasingly negative, it seems likely that a point will be reached at which convective instability will assume the dominant role. In order to examine the relative roles played by these two kinds of instability it is convenient to simplify the model to permit simpler parameterization. We therefore let $R_1 = R_2 = (N_3/\beta)^2 = \delta = 0$. The static stability, shear and orientation are then represented in the single parameter $(N_1/\beta)\,(m/k)$. There is thus an equivalency between static instability N_1/β and disturbance orientation m/k, and the results we will present may be interpreted in terms of either parameter. However, it must be remembered that m/k appears also in the dependent variable $\xi = C/\Delta u = (\sigma/\beta\alpha)\,(m/k)$ in Eqs. (20) and (21). We have chosen to parameterize the results shown in Fig. 12 in terms of orientation of the disturbance, assuming $(N_1/\beta)^2 = -0.05$. The figure can also be used to describe the results in terms of $(N_1/\beta)^2$, assuming $m/k = 1$, if the values of $(\sigma/\beta)_{r,i}$ for each curve in the figure are multiplied by their indicated m/k. Then the curves in increasing order of the indicated m/k correspond to $(N_1/\beta)^2 = -0.05, -0.45, -1, -1.8, -5$, respectively.

In Fig. 12, loci of pure-real roots are labeled "real." All others are complex, with the imaginary part plotted above zero on the σ/β scale and the real part plotted below. Because $R = 0$, only the right-hand branch of the hyperbola-like real roots (see Fig. 3) are seen in Fig. 12a.

There are several points of interest in Fig. 12:

1) As m/k varies, two regions are evident. One region, shown in Fig. 12a, has a set of roots exhibiting a rather well-defined most-unstable scale. These roots represent dynamic instability and in this region of m/k and α dynamic instability dominates. The band of unstable wavenumbers if fairly broad because $R = 0$. For $m/k = 1,3$ there is another set of roots whose loci in this region are nearly straight lines passing through the origin. These roots represent convective instability, and have no most unstable scale. In the region in Fig. 12b where $m/k \geq 4.5$, or $(N_1 m/\beta k)^2 \leq -1$, only roots for convective instability exist in this model. Here the instability increases steadily as α increases (scale size decreases). In reality, viscous damping would take over at some small scale size yielding a most unstable scale at some high wavenumber. Thus, there may be two initially most rapidly growing scales of disturbance: one dynamic and one convective, with the dynamic having a much larger scale size. It seems not unreasonable that the larger scale dynamic instability may sometimes be the trigger that initiates large deep convection.

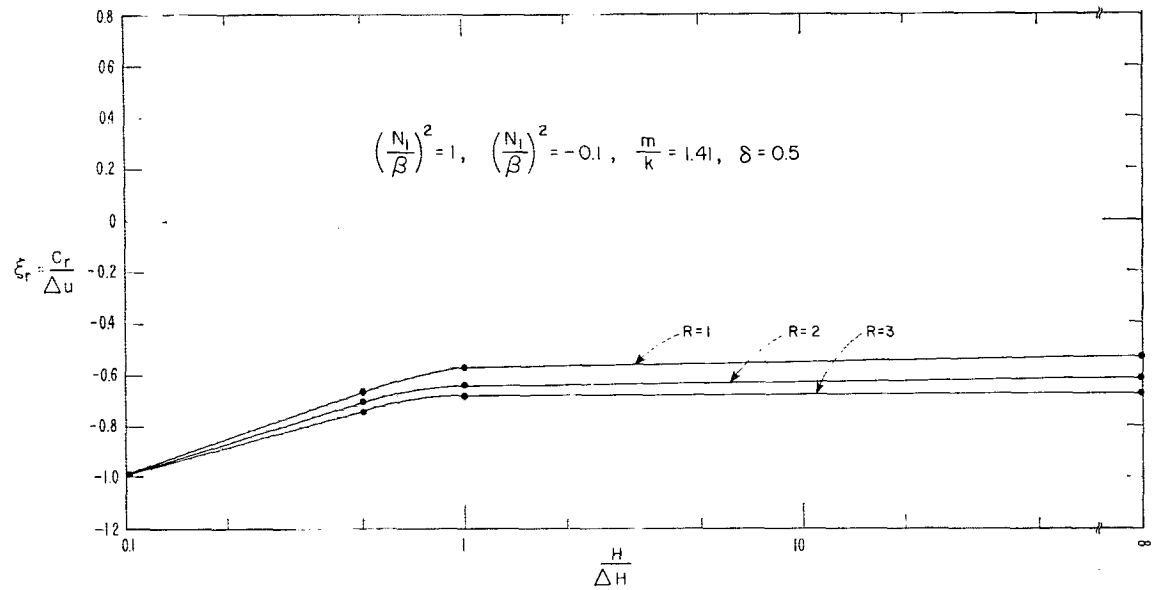

FIG. 8. Influence of the height of the base of the shear layer on the phase velocity of the most unstable disturbance: $C_r/\Delta u = -1$ when the velocity of the disturbance is 0 relative to the ground; $C_r/\Delta u = 0$ when the velocity of the disturbance is that of the wind at the center of the shear layer.

The real roots also exhibit a characteristic behavior in the two domains. In Fig. 12a, the right-hand branch of the hyperbola-like loci, typical of the real roots in Fig. 3, are to be seen at the lower right. At the value $m/k = 4.5$, where dynamic instability is cut off, the lower part of the hyperbola no longer bends back toward larger α, and in the convective domain (Fig. 12b) they loop in the origin. This conclusion is quite general and is not altered by letting N_3/β, R or δ be non-zero. However, if R' is not zero it is no longer true.

2) In the domain dominated by dynamic instability the most unstable configuration is a two-dimensional disturbance transverse to the shear ($m/k = 1$) and is probably the explanation of those cloud streets observed to be oriented transverse to the mean wind shear.

3) In the domain of convective instability the most unstable configuration is a two-dimensional disturbance aligned along the shear ($m/k = \infty$) and is probably the explanation of those cloud streets aligned along the mean wind shear.

4) Making $(N_1/\beta)^2$ more negative increases the convective instability but decreases the dynamic insta-

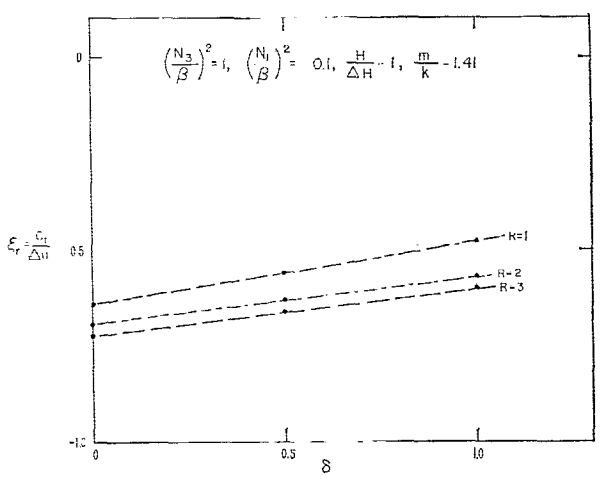

FIG. 9. Influence of wind and temperature discontinuity on the phase velocity of the most unstable disturbance. $\delta = \delta u/\Delta u$. For interpretation of ordinate scale, see caption for Fig. 8.

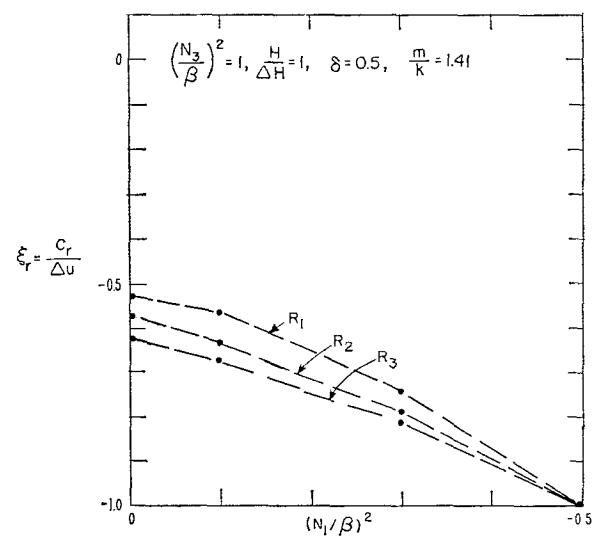

FIG. 10. Influence of intensity of superadiabatic layer on the phase velocity of the most unstable disturbance. For interpretation of ordinate scale, see caption for Fig. 8.

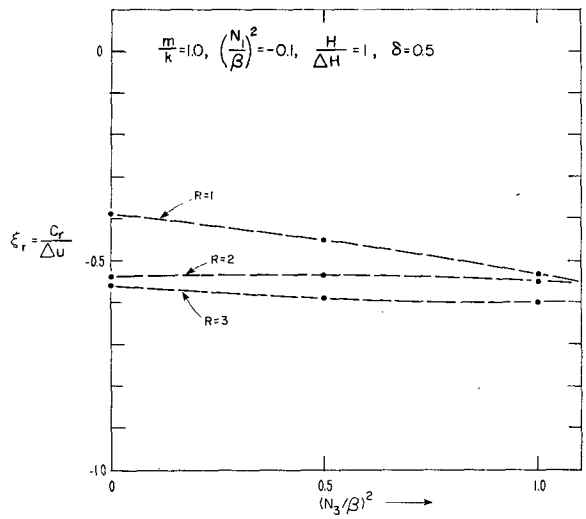

FIG. 11. Influence of static stability of the upper atmosphere on phase velocity of the most unstable disturbance for the two-dimensional model. For interpretation of left-hand scale see caption for Fig. 8.

bility until it is cut off for $(N_1 m/\beta k)^2 \leqslant -1$. Thus shear increases the dynamic instability while it stabilizes the convectively unstable modes. There are multiple solutions for the convective type of instability, representing higher order modes. In Fig. 12 we have shown only the most unstable roots of this type.

The conclusions above are remarkably similar to results obtained by Asai (1970) for a very different model. Asai chose a model with mean flow between parallel, free boundaries across which a linear, statically unstable temperature profile was assumed to exist. The profile of the mean flow, which had an inflection point, was described by $u_0(z)=\frac{1}{2}[1-(2z-1)^2]^n$, $n=1, 2, \ldots$. In contrast, our model has no shear across the statically unstable lower layer, within which the momentum is assumed to be intensely mixed, but instead the shear is across a statically neutral layer above. Furthermore, these two layers are capped with a statically stable region. Asai called the dynamically unstable domain "inertially unstable," and the convectively unstable domain "thermally unstable."

The four points listed above are not altered fundamentally when R and $(N_3/\beta)^2$ are not zero. The main effect of R is to narrow the band of dynamically unstable wavenumbers while leaving the convective domain virtually unchanged. The principal effect of increasing stability above the shear layer is to shift everything to the right along the α axis. For example, the most unstable wavenumber in the dynamically unstable domain is shifted toward larger wavenumbers much as shown in Fig. 4. The magnitude of the static instability at transition $[(N_1 m/\beta k)^2 = -1]$ does not vary with upper level stability, or $R \neq 0$, but the position of the transition shifts to the right on the α axis. At $\sigma/\beta=0$ the real root is at $\alpha=0.5$ when $(N_3/\beta)^2=0$, but is at $\alpha=0.72$ and 1.0, respectively, when $(N_3/\beta)^2$ is 0.45 and 1.0.

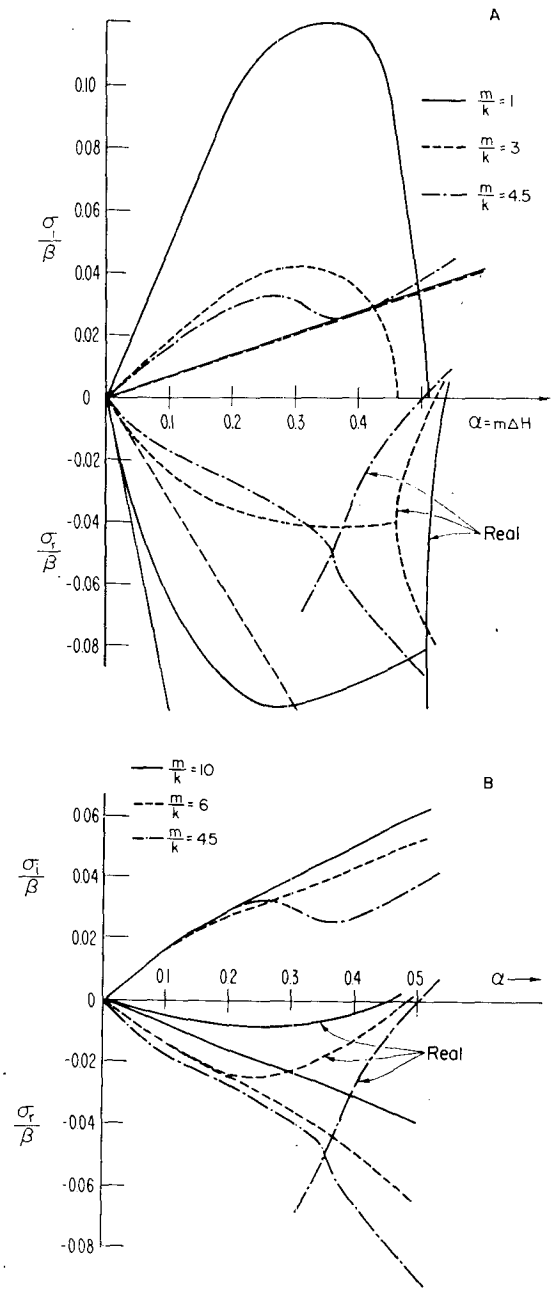

FIG. 12. Effect of orientation of perturbation on instability. Plots are the loci of roots for a model in which $H/\Delta H=1$, $(N_1/\beta)^2 = -0.05$, $R=R'=N_3/\beta=0$. Pure-real roots are labeled "real." The other curves are complex roots with the imaginary part plotted above zero on the σ/β axis and the real part is plotted below. The top frame shows the domain of m/k in which dynamic instability is dominant. The bottom frame shows the domain in which only convective instability exists. The curves can also be interpreted in terms of strength of static instability in the lower layer instead of orientation (see text). The four major conclusions to be drawn from this figure are listed in Section 6 in the subsection on convective instability and orientation.

7. Discussion

We have taken no account of transient conditions in our formulation of the problem because our goal was limited to finding the conditions for the onset of dynamic instability of infinitesimal disturbances. By the nature of the assumptions, such disturbances will initially grow exponentially with time. Much theoretical work has been done on the way the boundary layer evolves after sunrise. Recent papers in this category include those of Tennekes (1973), Stull (1973) and Carson (1973). These models have been concerned with the heat budget in the boundary layer as the day progresses, i.e., they consider the effects of solar heating of the surface, entrainment of air across the interfacial (capping) inversion, and (sometimes) subsidence, on the rate of increase in depth of the convective boundary layer. They do not explicitly include the effects of shear, advection, evaporation or (usually) radiation. In contrast, we explicitly focus on the effects of shear and the capping inversion, and we will only qualitatively consider how the developing boundary layer might create the inflection point in the wind profile needed to generate this kind of dynamic instability.

Thus one might imagine the following sequence of events to occur following sunrise. As the night ends, assume that the lower atmosphere is characterized by a surface-based shear layer such that the wind profile has no inflection points. Because shear always appears in dimensionless quantities along with the Väisälä-Brunt frequency N or the temperature discontinuity $\Delta\theta$, note that this kind of instability is possible even though the shear be made arbitrarily small— but not zero. As surface heating proceeds, an intensely mixed layer forms next to the ground, and the resulting large rate of transfer of momentum leads to a nearly constant wind throughout the lower layer (except, of course, in the constant flux layer next to the ground ignored in our model). The base of the shear layer is then approximately at the top of the intensely mixed layer, and the resulting inflection point in the profile leads to dynamic instability. This situation might resemble that shown in Fig. 2. As the base of the shear layer rises, the strength of the dynamic instability increases until a height of about $H=\Delta H$ is reached, after which there is little further increase. As it increases, the instability may become sufficient to overcome the frictional resistance in the system and large-scale perturbations may be initiated which will presumably modify the environment and invalidate the linearizing assumptions used in predicting the conditions for the initial onset of the instability. It is even possible that, if the lower atmosphere contains an adequate moisture supply and favorable mesoscale circulation, the perturbation may be sufficient to trigger the thermodynamic processes needed to bring about large deep convection associated with storms.

We should not expect the above eigenvalue relations or even the predicted kinematics of the flow to be valid later in the convective development when the inviscid and small perturbation assumptions no longer hold. However, with that disclaimer, we will proceed to calculate the flow patterns hoping the reader will exercise suitable caution in comparing them with real convective systems, especially near the critical level.

8. Flow patterns, vorticity, and divergence

The behavior of the flow patterns near the critical level in the three-dimensional, inviscid shear model is interesting. Infinities occur in U, V and vorticity at the critical level that are not found in two-dimensional models. To show this we first express all velocity components in terms of the perturbation in W at the top of the shear layer [i.e., $W_{H+2\Delta H}$ in Eqs. (18) and (19)]. Letting the total velocity $u_T=u_0(z)+U$, where u_0 is the unperturbed and U the perturbed component of the velocity in the x-direction, we find from Eqs. (13) and (14) that

$$u_T=u_0(z)-\frac{k}{m^2}\left(\frac{\partial}{\partial z}-\frac{k}{\omega}\beta\frac{l^2}{k^2}\right)W(z)\cos ly\sin(kx-\sigma t), \quad (22)$$

$$V=-\frac{l}{m^2}\left(\frac{\partial}{\partial z}+\frac{k}{\omega}\beta\right)W(z)\sin ly\cos(kx-\sigma t), \quad (23)$$

$$W=W(z)\cos ly\cos(kx-\sigma t), \quad (24)$$

where $W(z)$ is given by Eqs. (17)–(19). We again remind the reader that the origin of the height coordinate is at the center of the shear layer (see Fig. 1) so that in the shear layer $u_0(z)=\beta z$ where β is the shear factor— assumed here to be constant.

It is important to note that the 2nd term in the parentheses of Eqs. (22) and (23) becomes infinite where $\omega=0$. If ω is real, this occurs at the level where the disturbance velocity is equal to the environmental flow velocity, i.e., the critical level. Consequently, U and V there become infinite even though W and its height derivative do not and even though there are no singularities in the wave equation in W. This is a result of the three-dimensional nature of the model, as seen from the fact that when $l=0$, i.e., the wave propagates precisely in the direction of the shear vector, the terms in ω^{-1} drop out and the infinities disappear. They also disappear even in the three-dimensional case if there is no shear, i.e., $\beta=0$.

From (18) and (19) we can calculate the vorticity and divergence. In the horizontal plane, the vertical component of vorticity is

$$\mathrm{vor}_H=\frac{\partial V}{\partial x}-\frac{\partial u_T}{\partial y}=+\frac{\beta l}{\omega}W$$

and the divergence is

$$\mathrm{div}=\frac{\partial u_T}{\partial x}+\frac{\partial V}{\partial y}=-\frac{\partial W}{\partial z}$$

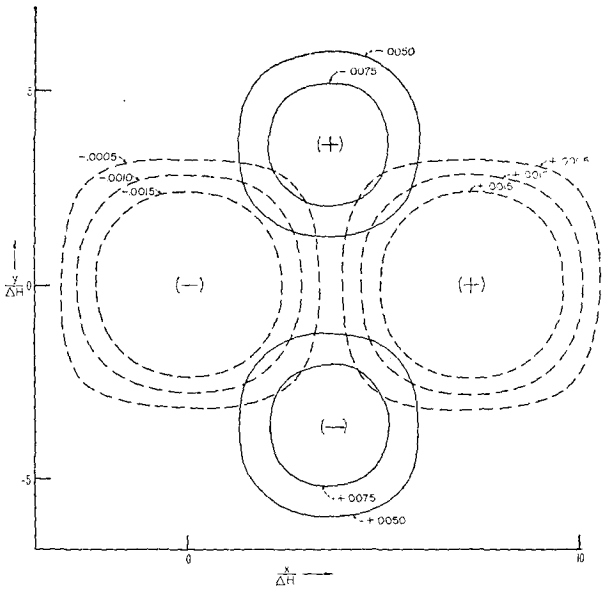

FIG. 13. Vorticity pattern (solid curves) and divergence pattern (dashed curves) at the base of the shear layer ($z/\Delta H=-1$) of a model in which $H/\Delta H=1$, $(N_3/\beta)^2=1$, $(N_1/B)^2=-0.1$, $k=l$, $\delta=1$, $R=1$ and $2\Delta u/W_H=4$. Then $\alpha_r=0.62$, $A=-1.21$ and the critical level is at a height of $z/\Delta H=-0.48$.

If ω is real, we see that vorticity becomes infinite at the critical level [unless $W(z)$ goes to zero as fast or faster than ω as $z\to z_c$] while divergence remains well behaved.

In the middle layer, where $\omega/\beta=(k\alpha/m)(\xi-z/\Delta H)$,

$$u_T=\beta z-\frac{k}{m}\left\{\frac{1}{m}\frac{\partial W(z)}{\partial z}-\frac{l^2}{k^2}\frac{W(z)}{\alpha\left(\xi-\dfrac{z}{\Delta H}\right)}\right\}\times\cos ly\sin(kx-\sigma t), \quad (25)$$

$$V=-\frac{l}{m}\left\{\frac{1}{m}\frac{\partial W(z)}{\partial z}+\frac{W(z)}{\alpha\left(\xi-\dfrac{z}{\Delta H}\right)}\right\}\times\sin ly\cos(kx-\sigma t), \quad (26)$$

$$\mathrm{vor}_H=-\left(\frac{l}{k}\right)\frac{W(z)}{\Delta H\left(\xi-\dfrac{z}{\Delta H}\right)}\sin ly\sin(kx-\sigma t), \quad (27)$$

where

$$W(z)=W_{H+2\Delta H}\frac{\sinh mz+A\cosh mz}{\sinh m\Delta H+A\cosh m\Delta H}, \quad (28)$$

$$\frac{\partial W}{\partial z}=m\frac{\cosh mz+A\sinh mz}{\sinh m\Delta H+A\cosh m\Delta H}W_{H+2\Delta H}. \quad (29)$$

It is readily seen from Eq. (27) that the presence of a critical level has an important effect on vorticity when

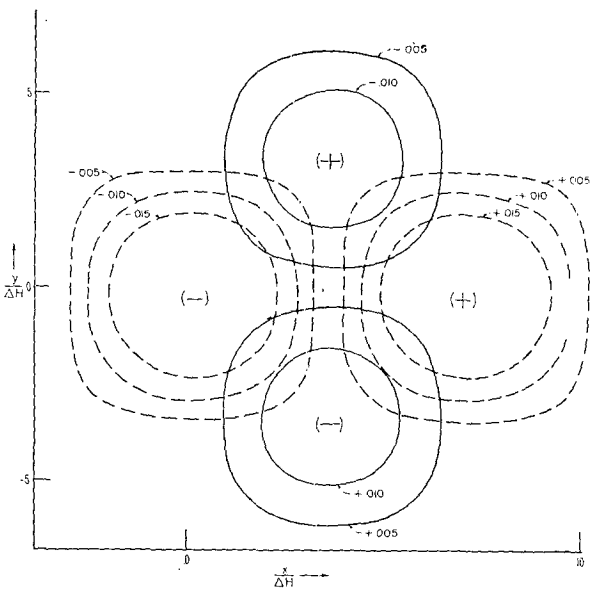

FIG. 14. As in Fig. 12 except $z/\Delta H=-0.8$.

1) the disturbance is three-dimensional and 2) vertical shear exists in the background wind. If the disturbance is two-dimensional ($l=0$), or if there is no shear ($\Delta u=0$, $\xi=\infty$), $\mathrm{vor}_H=0$ in this model. Contours of vorticity (solid curves) and divergence in four horizontal planes bracketing the critical level (taken to be at $z/\Delta H=-0.48$) are shown in Figs. 12–16. At the critical level the vorticity becomes infinite and reverses sign, but in the real atmosphere both viscosity and nonlinear effects must have an important influence at this level. However, in spite of the defects associated with the linear theory, it seems clear that vorticity can occur in such three-dimensional systems even when large-scale

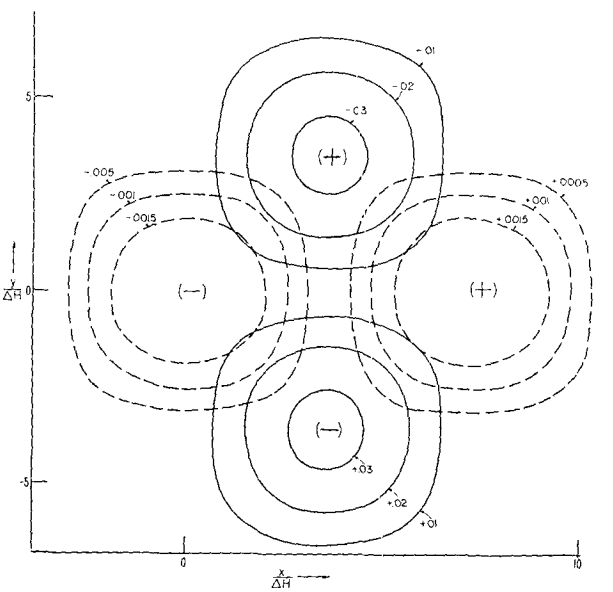

FIG. 15. As in Fig. 12 except $z/\Delta H=-0.6$.

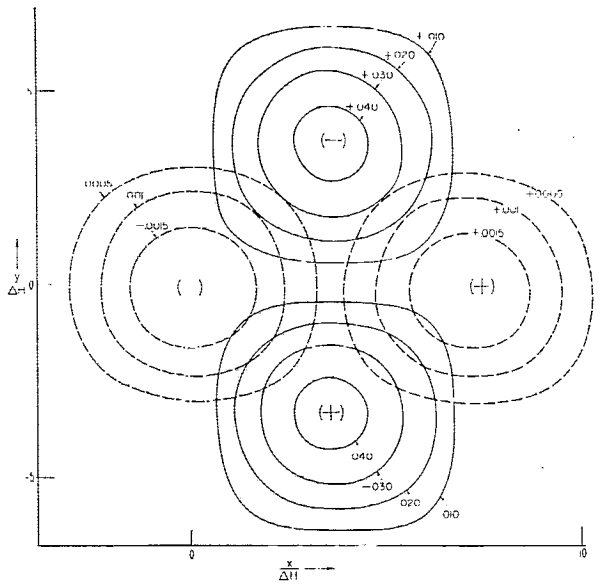

FIG. 16. As in Fig. 12 except $z/\Delta H = -0.4$.

horizontal gradients of velocity are absent and without any particular concentration of vorticity in the background flow by the disturbance itself.

9. Conclusions

We have analyzed the dynamic stability and kinematics of a sheared convective boundary layer capped by a temperature and wind discontinuity; a neutral or unstable surface layer lies beneath an adiabatic layer under shear. We find that the capping inversion can lead to a narrow band of unstable wavenumbers that depends on shear layer thickness. The bandwidth and propagation speed of these "most unstable" scales is closely related to the height of the shear layer above the surface. In fact, the width of the band of instability shrinks to zero when the shear layer becomes surface-based or when the intensity of the thermal instability of the lower layer becomes high. The static stability above the shear layer determines what scales of disturbance can leak their energy away from the shear layer by internal gravity wave propagation into the upper atmosphere, because it determines the position of the long-dashed lines in Fig. 3.

Whereas there is a most unstable wavelength associated with dynamic instability, convective instability is greater the higher the wavenumber, in the absence of viscosity; so dynamic instability will tend to be dominant at the larger scales. The shear needed to produce dynamic instability actually reduces the magnitude of the convective instability. Two-dimensional disturbances aligned transverse to the wind shear are most dynamically unstable, while two-dimensional rolls aligned along the wind shear are most convectively unstable.

We have shown that the kinematics and vorticity of initially "most-unstable," three-dimensional disturbances under shear depend importantly on the presence of a critical level within the growing disturbance. Infinities occur in the three-dimensional, inviscid shear models that do not occur in the two-dimensional models.

Acknowledgments. We wish to express our appreciation to Dr. Franco Einaudi for giving us his modified version of the Lewis algorithm used in searching the complex plane, and for helpful discussions. We wish also to thank Drs. Stanley Barnes, Dan Fitzjarrald, William Hooke, James Deardorff, and Tzvi Gal-Chen for reading the manuscript and offering suggestions.

REFERENCES

Asai, Tomio, 1970: Stability of a plane parallel flow with variable vertical shear and unstable stratification. *J. Meteor. Soc. Japan*, **48**, 129–139.

Booker, J. R., and F. P. Bretherton, 1967: The critical layer for internal gravity waves in a shear flow. *J. Fluid Mech.*, **27**, 513–539.

Brown, R. A., 1970: A secondary flow model of the planetary boundary layer. *J. Atmos. Sci.*, **27**, 742–757.

——, 1972: On the inflection point instability of a stratified Ekman boundary layer. *J. Atmos. Sci.*, **29**, 850–859.

Brunt, D., 1927: The period of simple vertical oscillations in the atmosphere. *Quart. J. Roy. Meteor. Soc.*, **53**, 30–32.

Carson, J. D., 1973: The development of a dry inversion-capped convectively unstable boundary layer. *Quart. J. Roy. Meteor. Soc.*, **99**, 450–467.

Case, K. M., 1960: Stability of inviscid plane Couette flow. *Phys. Fluids*, **3**, 143–148.

Deardorff, J. W., 1965: Gravitational instability between horizontal plates with shear. *Phys. Fluids*, **8**, 1027–1030.

Gallagher, A. P., and A. McD. Mercer, 1965: On the behaviour of small disturbances in plane Couette flow with a temperature gradient. *Proc. Roy. Soc. London*, **A286**, 117–128.

Goldstein, S., 1931: On the stability of superposed streams of fluid of different densities. *Proc. Roy. Soc. London*, **A132**, 524–548.

Gossard, Earl E., 1974: Dynamic stability of an isentropic shear layer in a statically stable medium. *J. Atmos. Sci.*, **31**, 483–492.

——, and William H. Hooke, 1975: *Waves in the Atmosphere*. Amsterdam, Elsevier 480 pp.

Hazel, Philip, 1967: The effect of viscosity and heat conduction on internal gravity waves at a critical level. *J. Fluid Mech.*, **30**, 775–783.

Holmboe, J., 1962: On the behavior of symmetric waves in stratified shear layers. *Geophys. Publ.*, **24**, No. 2, 68–113.

Howard, L. N., 1963: Neutral curves and stability boundaries in stratified flow. *J. Fluid Mech.*, **16**, 333–342.

Kaylor, R., and A. Faller, 1972: Instability of the stratified Ekman boundary layer and the generation of internal waves. *J. Atmos. Sci.*, **29**, 497–509.

Kelvin, Lord, 1880: On a disturbing infinity in Lord Rayleigh's solution for waves in a plane vortex stratum. *Nature*, **33**, 45–46.

Kuo, H. L., 1963: Perturbations of plane Couette flow in a stratified fluid and origin of cloud streets. *Phys. Fluids*, **6**, 195–211.

LeMone, M. A., 1973: The structure and dynamics of horizontal roll vortices in the planetary boundary layer. *J. Atmos. Sci.*, **30**, 1977–1091.

Lewis, L. D., 1966: U. S. Department of Commerce, NOAA/ERL/SEL unpublished computer subroutine.

Lilly, D. K. 1966: On the instability of Ekman boundary flow. *J. Atmos. Sci.*, **23**, 481–494.

Maslowe, S. A., and J. Thompson, 1971: Stability of a stratified free shear layer. *Phys. Fluids*, **14**, 453–458.

Moninger, W. R., 1974: The search for most unstable scales of disturbances in three-layer atmospheric models with shear and static stability—procedure and results. NOAA Tech. Rept. ERL 314-WPL 36.

Ramm, Pauline, and F. W. G. Warren, 1963: Gravity-wave dispersion under wind shear in two model atmosphere. *Quart. J. Roy. Meteor. Soc.*, **89**, 349–359.

Stull, R. B., 1973: Inversion rise model based on penetrative convection. *J. Atmos. Sci.*, **30**, 1092–1099.

Taylor, G. E., 1931: Effect of variation in density on the stability of superposed streams of fluid. *Proc. Roy. Soc. London*, **A132**, 499–523.

Tennekes, H., 1973: A model for the dynamics of the inversion above a convective boundary layer. *J. Atmos. Sci.*, **30**, 558–567.

Väisälä, V., 1925: Uber die Wirkung der Windschwankungen auf die Pilot-Beobachtungen. *Soc. Sci. Fenn. Commentat. Phys.-Math.*, **2**, 2–46.